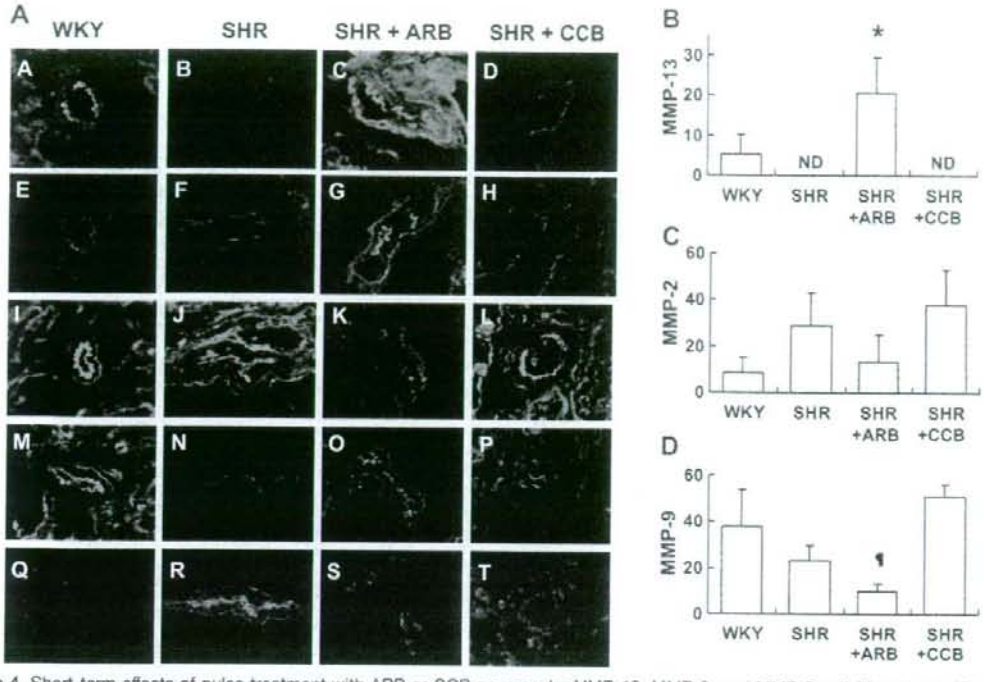

Figure 4. Short-term effects of pulse treatment with ARB or CCB on vascular MMP-13, MMP-2, and MMP-9 activities at age 18 weeks in SHRs. A, Representative in situ zymograms of (A through D) total type I collagenolytic activity; (E through H) type I collagenolytic activity in the presence of MMP-13 inhibitor; (I through L) total type IV collagenolytic activity; (M through P) type IV collagenolytic activity in the presence of MMP-2 inhibitor; and (Q through T) type IV collagenolytic activity in the presence of MMP-9 inhibitor. B through D, Quantification of (B) MMP-13, (C) MMP-2, and (D) MMP-9 activities in medial layers of renal arterioles. Abbreviations of groups as in Figure 2. *$P<0.05$ vs WKY rats; ¶$P<0.05$ vs SHR + CCB.

pulse treatment with different doses of ARB (1 to 50 mg/kg per day) on regression of glomerular hypertrophy and sclerosis and have found that the maximal effect on the regression of glomerular changes is obtained with the high dose (50 mg/kg per day) used in this study (unpublished observation).

One caveat of this study concerns the limitations of the indirect measurement of blood pressure. As in our previous studies, we performed the blood pressure measurements of the different groups on the same day, with the same experienced investigator, after an initial period of training under

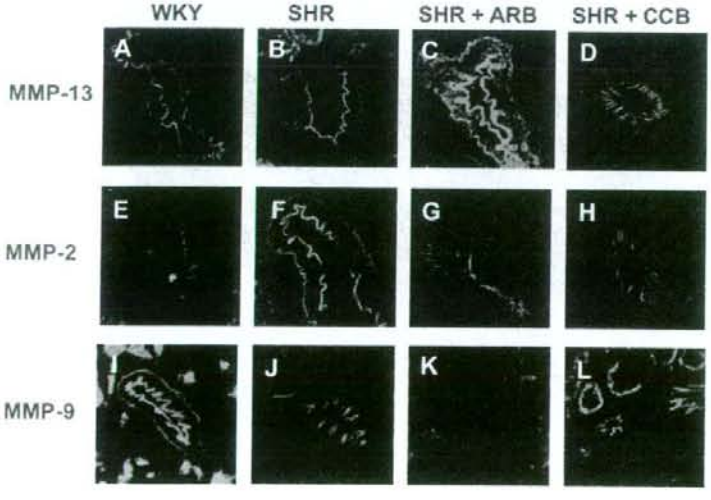

Figure 5. Short-term effects of pulse treatment with ARB or CCB on vascular MMP-13, MMP-2, and MMP-9 expression at age 18 weeks in SHRs. Immunofluorescent staining of (A through D) MMP-13 protein; (E through H) MMP-2 protein; and (I through L) MMP-9 protein.

stress-free conditions. Under these conditions, we found a clear-cut reduction of blood pressure (>30 to 40 mm Hg) in the ACEI- and ARB-treated groups every 2 weeks, consistently over several months, compared with the control, CCB-treated, and vasodilator-treated groups. However, it should be recognized that the indirect method is less accurate than direct measurement using an indwelling catheter, and absolute values of blood pressure may not be wholly reliable.[13] Moreover, unlike the telemetry method, the measurements were made at a single point and were not made continuously over multiple days; thus, small differences in blood pressure between the different groups at age 18 weeks cannot be accurately assessed. Because of the limited precision of the tail-cuff method, we cannot conclude whether the effects of ARB at age 18 weeks are entirely independent of blood pressure.

An important finding was that treatment with a high dose of ARB alone was sufficient to cause a remarkable reversal of renal arteriolar hypertrophy in the course of just 2 weeks. The media:lumen ratios of the small renal arterioles in the ARB pulse-treated rats were decreased almost to the levels found in the normotensive WKY rat, whereas the CCB did not have a significant effect. Several lines of evidence suggest that hypertrophy of the small arterioles in the kidney plays a major role in the pathogenesis of hypertension in the SHR.[10,11,14] Therefore, the observed reversal of renal arteriolar hypertrophy is compatible with the regression of hypertension seen in the ARB-treated groups.

Because we found marked changes in the kidney after just 2 weeks of pulse treatment, we performed a comprehensive survey (microarray analysis) of the differences in gene expression in the kidney of ARB-treated and CCB-treated rats. Interestingly, the microarray analysis did not reveal a major change in components of the RAS, except for an increase in renin mRNA, which could be expected as a feedback response to RAS inhibition. In contrast, expression of several extracellular matrix–related proteins, in particular, MMPs and TIMPs, was differently affected by the 2 treatments, and these results were confirmed by RT-PCR analysis. We focused on these findings, because changes in the expression of these genes could be involved in the remodeling of the renal arterioles. To clarify the changes in the renal arterioles, we assayed tissue MMP activity using a recently developed high-resolution, high-sensitivity in situ zymography technique.[12] Using this method, we found that the ARB treatment had different effects on the vascular MMP system than the CCB treatment and caused an increase in vascular MMP-13 activity and a decrease in MMP-9 activity, which could explain the different effects on regression of renal arteriolar hypertrophy. These findings were confirmed immunohistologically, by immunofluorescence staining of these MMPs.

It is well established that the MMPs, in particular, members of the collagenase and gelatinase families, play an important role in tissue remodeling by cleaving many structural proteins of the extracellular matrix.[15] MMP-13 is the predominant collagenase in rodents that lack the gene for MMP-1 and is involved in the collagenolysis of types I, II, and III collagens.[16] MMP-13 is known to be expressed in cultured vascular smooth muscle cells[17] and has been implicated in remodeling of the uterine artery during pregnancy,[18] in angiogenesis,[19] and in aneurysm formation.[17] These reports are consistent with the notion that upregulation of vascular MMP-13 activity by high-dose ARB in this model will result in collagenolysis of vascular collagens, favoring regression of renal arteriolar hypertrophy. It has been reported that MMP-9 (gelatinase B) is also expressed in cultured vascular smooth muscle cells, where it is involved in cell migration[20] and is upregulated by angiotensin II.[21] Therefore, the inhibition of MMP-9 by ARB could cause inhibition of compensatory smooth muscle cell migration, further contributing to the vascular changes.

The results of this study extend the work of Smallegange et al[9] using ACEI and a low-salt diet. In their studies, they found that cross-transplantation of kidneys from rats treated transiently with ACEI and a low-salt diet to hypertensive rats caused a transfer of the sustained reduction of blood pressure, whereas the untreated kidneys caused an increase in blood pressure. Moreover, the ACEI and low-salt treatment caused a significant decrease in renal vascular resistance. We speculate that the marked regression of renal small arteriolar hypertrophy ("renal microvascular remodeling") reported in this study is intimately involved in the mechanism of hypertension regression found in these models.

Perspectives

Because the animal studies on the prevention of hypertension development were successfully confirmed clinically by the Trial of Preventing Hypertension,[8] we have now designed a multicenter prospective clinical study (Short Treatment With Angiotensin Receptor Candesartan Surveyed by Telemedicine Study) to examine the feasibility of regression of established hypertension (ie, reversal from stage 1 to prehypertension) using transient ARB treatment in patients with essential hypertension.[22] The results of this study lead us to speculate that the development of methods to cause regression (or cure) of hypertension, and the study of the mechanisms of regression, may become one of the central themes in hypertension research this century.

Acknowledgment

We are grateful to Dr Norman M. Kaplan, Southwestern Medical Center, for helpful discussion and comments about this article.

Sources of Funding

This work was supported by grants 20590984, 17590844, and 18790578 from the Ministry of Education, Culture, Science and Technology, Japan.

Disclosures

None.

References

1. Kearney PM, Whelton M, Reynolds K, Muntner P, Whelton PK, He J. Global burden of hypertension: analysis of worldwide data. *Lancet*. 2005; 365:217–223.
2. Lawes CM, Vander Hoorn S, Rodgers A. Global burden of blood-pressure-related disease, 2001. *Lancet*. 2008;371:1513–1518.
3. Harrap SB, Van der Merwe WM, Griffin SA, Macpherson F, Lever AF. Brief angiotensin converting enzyme inhibitor treatment in young spon-

taneously hypertensive rats reduces blood pressure long-term. *Hypertension*. 1990;16:603–614.
4. Richer C, Mulder P, Fornes P, Richard V, Camilleri JP, Giudicelli JF. Hemodynamic and morphological effects of quinapril during genetic hypertension development. *J Cardiovasc Pharmacol*. 1991;18:631–642.
5. Nakaya H, Sasamura H, Hayashi M, Saruta T. Temporary treatment of prepubescent rats with angiotensin inhibitors suppresses the development of hypertensive nephrosclerosis. *J Am Soc Nephrol*. 2001;12:659–666.
6. Nakaya H, Sasamura H, Mifune M, Shimizu-Hirota R, Kuroda M, Hayashi M, Saruta T. Prepubertal treatment with angiotensin receptor blocker causes partial attenuation of hypertension and renal damage in adult Dahl salt-sensitive rats. *Nephron*. 2002;91:710–718.
7. Ishiguro K, Sasamura H, Sakamaki Y, Itoh H, Saruta T. Developmental activity of the renin-angiotensin system during the "critical period" modulates later L-NAME-induced hypertension and renal injury. *Hypertens Res*. 2007;30:63–75.
8. Julius S, Nesbitt SD, Egan BM, Weber MA, Michelson EL, Kaciroti N, Black HR, Grimm RH Jr, Messerli FH, Oparil S, Schork MA. Feasibility of treating prehypertension with an angiotensin-receptor blocker. *N Engl J Med*. 2006;354:1685–1697.
9. Smallegange C, Hale TM, Bushfield TL, Adams MA. Persistent lowering of pressure by transplanting kidneys from adult spontaneously hypertensive rats treated with brief antihypertensive therapy. *Hypertension*. 2004;44:89–94.
10. Skov K, Mulvany MJ. Structure of renal afferent arterioles in the pathogenesis of hypertension. *Acta Physiol Scand*. 2004;181:397–405.
11. Gattone VH, II, Evan AP, Willis LR, Luft FC. Renal afferent arteriole in the spontaneously hypertensive rat. *Hypertension*. 1983;5:8–16.
12. Ahmed AK, Haylor JL, El Nahas AM, Johnson TS. Localization of matrix metalloproteinases and their inhibitors in experimental progressive kidney scarring. *Kidney Int*. 2007;71:755–763.
13. Ibrahim J, Berk BC, Hughes AD. Comparison of simultaneous measurements of blood pressure by tail-cuff and carotid arterial methods in conscious spontaneously hypertensive and Wistar-Kyoto rats. *Clin Exp Hypertens*. 2006;28:57–72.
14. Feihl F, Liaudet L, Levy BI, Waeber B. Hypertension and microvascular remodelling. *Cardiovasc Res*. 2008;78:274–285.
15. Sasamura H, Shimizu-Hirota R, Saruta T. Extracellular matrix remodeling in hypertension. *Curr Hypertens Rev*. 2005;1:51–60.
16. Woessner JF Jr. Matrix metalloproteinases and their inhibitors in connective tissue remodeling. *FASEB J*. 1991;5:2145–2154.
17. Mao D, Lee JK, VanVickle SJ, Thompson RW. Expression of collagenase-3 (MMP-13) in human abdominal aortic aneurysms and vascular smooth muscle cells in culture. *Biochem Biophys Res Commun*. 1999; 261:904–910.
18. Kelly BA, Bond BC, Poston L. Gestational profile of matrix metalloproteinases in rat uterine artery. *Mol Hum Reprod*. 2003;9:351–358.
19. Zijlstra A, Aimes RT, Zhu D, Regazzoni K, Kupriyanova T, Seandel M, Deryugina EI, Quigley JP. Collagenolysis-dependent angiogenesis mediated by matrix metalloproteinase-13 (collagenase-3). *J Biol Chem*. 2004;279:27633–27645.
20. Yu YM, Lin HC, Chang WC. Carnosic acid prevents the migration of human aortic smooth muscle cells by inhibiting the activation and expression of matrix metalloproteinase-9. *Br J Nutr*. 2008:1–8.
21. Guo RW, Yang LX, Li MQ, Liu B, Wang XM. Angiotensin II induces NF-kappa B activation in HUVEC via the p38MAPK pathway. *Peptides*. 2006;27:3269–3275.
22. Sasamura H, Nakaya H, Julius S, Takebayashi T, Sato Y, Uno H, Takeuchi M, Ishiguro K, Murakami M, Ryuzaki M, Itoh H. Short treatment with the angiotensin receptor blocker candesartan surveyed by telemedicine (STAR CAST) study: rationale and study design. *Hypertens Res*. 2008;31:1851–1857.

ONLINE SUPPLEMENT

'PULSE' TREATMENT WITH HIGH-DOSE ANGIOTENSIN BLOCKER REVERSES RENAL ARTERIOLAR HYPERTROPHY AND REGRESSES HYPERTENSION

Kimiko Ishiguro*, Kaori Hayashi*, Hiroyuki Sasamura, Yusuke Sakamaki, Hiroshi Itoh

Department of Internal Medicine, School of Medicine, Keio University, Tokyo, Japan

Correspondence to:

Hiroyuki Sasamura MD PhD

Department of Internal Medicine, School of Medicine, Keio University

35 Shinanomachi, Shinjuku-ku, Tokyo 160-8582, Japan

Tel: 81-3-5363-3796

Fax:81-3-3359-2745

E-mail: sasamura@sc.itc.keio.ac.jp

Running Title: Pulse ARB treatment in SHR

* These authors contributed equally to this study

Word counts: Manuscript 4334 words, Abstract 229 words

Group Number Treatment	1 WKY	2 SHR	3 SHR+ARB	4 SHR+CCB
Renal arterioles (30-100 um)	29.6±3.8	67.8±4.4*	36.5±4.2†	62.3±2.8*
Renal arterioles (100-300 um)	29.3±1.7	39.0±2.3	37.6±5.7	41.2±5.6
Mesenteric arterioles (30-100 um)	19.0±3.3	21.2±2.1	16.2±2.0	17.2±1.1
Mesenteric arterioles (100-300 um)	22.3±3.4	22.0±3.0	20.6±5.8	18.1±2.3
Cardiac arterioles (30-100 um)	17.5±3.4	24.9±2.1	20.1±1.9	25.1±2.0
Cardiac arterioles (100-300 um)	16.9±1.1	22.4±3.0	21.3.±1.6	25.4±1.0
Cerebral arterioles (30-100 um)	16.5±2.1	21.1±3.1	18.0±3.0	18.7±1.4
Cerebral arterioles (100-300 um)	16.1±1.9	19.9±3.0	21.4.±3.0	20.4±1.0

*: $p<0.01$ vs WKY ; † $p<0.01$ vs SHR

Online Supplement Table S1. Values of media/lumen ratios (x 100) of arterioles in the kidney, mesentery, heart, and brain in the different groups at age 18 weeks in Experiment 2. Results shown are means ± SEM. WKY: untreated WKY, SHR: untreated SHR, SHR+ARB: SHR treated with 'pulse' candesartan, SHR+CCB: SHR treated with 'pulse' nifedipine.

Relation of Blood Pressure Quantitative Trait Locus on Rat Chromosome 1 to Hyperactivity of Rostralventrolateral Medulla

Kamon Iigaya, Hiroo Kumagai, Toru Nabika, Yuji Harada, Hiroshi Onimaru, Naoki Oshima, Chie Takimoto, Tadashi Kamayachi, Takao Saruta, Hiroshi Itoh

Abstract—Genetic factors that induce essential hypertension have been examined using genome-wide linkage analyses. A quantitative trait locus (QTL) region that is closely linked to hypertension has been found on chromosome 1 in stroke-prone spontaneously hypertensive rats (SHRSPs). We used 2 congenic rats in which the blood pressure QTL on rat chromosome 1 was introgressed from SHRSP/Izm to Wistar-Kyoto (WKY)/Izm (WKYpch1.0) and from WKY/Izm to SHRSP/Izm (SHRSPwch1.0) rats by repeated backcrossing. Previous studies reported that the intermediate phenotype of this QTL for hypertension is characterized by the hyperactivity of the sympathetic nervous system in response to physiological and psychological stress. We performed intracellular patch-clamp recordings of rostral ventrolateral medulla (RVLM) neurons from WKY, WKYpch1.0, SHRSPwch1.0, and SHRSPs and compared the basal electrophysiological activities of RVLM neurons and the responses of these neurons to angiotensin II. The basal membrane potential of RVLM neurons from WKYpch1.0 was significantly "shallower" than that of the neurons from WKY. The depolarization of RVLM neurons from WKYpch1.0 in response to angiotensin II was significantly larger than that in neurons from WKY rats, whereas the depolarization of RVLM neurons from SHRSPwch1.0 was significantly smaller than that in neurons from SHRSPs. The response to angiotensin II of RVLM neurons from WKYpch1.0 and SHRSPs was sustained even after the blockade of all of the synaptic transmissions using tetrodotoxin. The QTL on rat chromosome 1 was primarily related to the postsynaptic response of RVLM bulbospinal neurons to brain angiotensin II, whereas both the QTL and other genomic regions influenced the basal activity of RVLM neurons. **(*Hypertension*. 2009;53:42-48.)**

Key Words: sympathetic nervous system ■ congenic rat ■ angiotensin II ■ stress ■ RVLM neurons

The stroke-prone spontaneously hypertensive rat (SHRSP) is a useful model for the study of human essential hypertension.[1] Previous genome-wide analyses identified a potent quantitative trait locus (QTL) on rat chromosome 1 (Chr-1) that is responsible for hypertension in SHRSPs; this trait was confirmed in congenic strains for the QTLs.[2–5] Further analyses of the congenic strains suggested that this QTL harbored a gene (or genes) that regulated sympathetic responses to various stresses, such as restraint, cold, and air-jet stress.[5–7] Because the stressors used were either physical or emotional in nature, we hypothesized that a common pathway regulating sympathetic responses to stress might be responsible for this phenomenon. In this regard, the genetic effects of the Chr-1 QTL on the neuronal activity of the rostral ventrolateral medulla (RVLM), which is thought to determine the basal sympathetic nervous tone in response to various inputs from higher brain centers,[8,9] were explored in this study. In addition, among various modulators of RVLM activity, we particularly focused on the role of angiotensin II (Ang II) based on the following observations: physiological studies on rabbits showed that cardiovascular responses to air-jet stress were attenuated by the infusion of Ang II receptor blockers into the RVLM, implying a pivotal role of angiotensinergic neurons in the RVLM on the responsiveness to emotional stress.[10] Thus, we studied the stimulatory effect of Ang II on RVLM neurons in a previous study using brain stem-spinal cord preparations from neonatal rats.[11]

In the present study, we used reciprocal congenic strains constructed to evaluate the effect of the blood pressure QTL on Chr-1 on the electrophysiological activities of RVLM neurons in the absence of any influence from blood pressure and the higher brain center in the hypothalamus. The basal activity and response to Ang II superfusion were recorded in a single neuron using the whole-cell patch-clamp technique.

Received June 10, 2008; first decision June 28, 2008; revision accepted October 28, 2008.

From the Division of Endocrinology, Metabolism, and Nephrology (K.I., N.O., C.T., T.K., T.S., H.I.), Department of Internal Medicine, Keio University School of Medicine, Tokyo; Department of Nephrology (H.K.), National Defense Medical College, Tokorozawa, Saitama; Department of Pathology (T.N., Y.H.), Shimane University School of Medicine, Izumo; and Department of Physiology (H.O.), Showa University School of Medicine, Tokyo, Japan.

Correspondence to Kamon Iigaya, Discipline of Physiology, F13, University of Sydney, New South Wales 2006, Australia. E-mail kamon@physiol.usyd.edu.au

Hypertension **is available at http://hyper.ahajournals.org** **DOI: 10.1161/HYPERTENSIONAHA.108.117804**

Materials and Methods

Animals

Two congenic rat strains, WKY.SHRSP-(D1Wox29-D1Arb21)/Izm (abbreviated as WKYpch1.0) and SHRSP.WKY-(D1Wox29-D1Arb21)/Izm (abbreviated as SHRSPwch1.0) were provided through the National BioResource Project for the Rat.[12] These strains were established by introgressing the chromosomal segment from SHRSP/Izm into Wistar-Kyoto (WKY)/Izm rats and vice versa.[5,13] The congenic region between D1Wox29 and D1Arb21 covered a 100:1 CI for the blood pressure QTL. The genotyping of >150 simple sequence-length markers confirmed that the background genome was homozygous for the original WKY and SHRSPs in the WKYpch1.0 and SHRSPwch1.0 strains, respectively.[3,5] Information on the congenic strains is available at the Web site of the National BioResource Project for the Rat (http://www.anim.med.kyoto-u.ac.jp/nbr/home.htm).

WKY/Izm and SHRSP/Izm rats were provided by the Disease Model Cooperative Research Association (Kyoto, Japan). The genomic constructs of the 4 strains used in this study are shown in References 4 and 5. The congenic rats were maintained in the Keio University School of Medicine Animal Laboratory Center. All of the rats were fed a standard laboratory chow and tap water ad libitum and kept in a room maintained at a constant temperature of 25°C. The experimental protocols were approved by the Keio University School of Medicine Animal Research Committee, in compliance with Japanese Law (No. 105).

Recording of Electrophysiological Activities

Experiments were performed on brain stem-spinal cord preparations obtained from 0- to 4-day-old rats. Under deep ether anesthesia, the brain stem and spinal cord were isolated and sectioned at the second thoracic nerve root (Th_2) level, as described previously.[11,14,15] The preparation was continuously superfused at 2 to 3 mL/min with a standard solution consisting of (in mmol/L) 124.0 NaCl, 5.0 KCl, 2.4 $CaCl_2$, 1.3 $MgCl_2$, 26.0 $NaHCO_3$, 1.2 KH_2PO_4, and 30.0 D-glucose and equilibrated with 95% O_2 and 5% CO_2 (pH7.4), at 26°C to 27°C.

Intracellular recordings using the whole-cell patch-clamp technique were performed as follows: a patch electrode was filled with the following pipette solution (mmol/L): 130 K-gluconate, 10 EGTA, 10 HEPES, 2 Na_2-ATP, 1 $CaCl_2$, 1 $MgCl_2$, and 0.5% lucifer-yellow (Aldrich Chemical [pH 7.2 to 7.3], adjusted with KOH). A patch-clamp amplifier (Axopatch 1D, Axon Instruments) was used to record the membrane potential. Before starting the intracellular recordings, the firing patterns were checked using extracellular recordings. RVLM neurons exhibiting discharges that were synchronized with the simultaneously recorded phrenic nerve activity were assumed to be respiratory neurons and were excluded from the study. The membrane potential was recorded using the current-clamp technique (20-pA increments from −100 to 20 pA, 500-ms duration) and was corrected for the junctional potential at the tip of the pipettes (−11 mV). The basal membrane potential and the firing rate were recorded over 10 minutes. The input resistance was calculated from the current-voltage curve. The membrane potential was shifted to −50 mV because of the negative current. One RVLM neuron per preparation was used in the experiment.

To evaluate the responses to Ang II, we superfused the brain stem-spinal cord preparation for 20 minutes with Ang II (6 μmol/L, Sigma-Aldrich) dissolved in a standard solution and recorded the changes in the membrane potential and in the input resistance of the RVLM neurons. Li and Guyenet[16] used a bath application of 0.3 to 1.0 μmol/L of Ang II in their slice preparations. In an earlier study from our laboratory, we used 1, 3, and 12 μmol/L of Ang II to examine the dose responsiveness of RVLM neurons in a brain stem-spinal cord preparation, in which the target neurons were located 100 μm from the surface of the preparation.[11] Based on these results, we selected the dosage of 6 μmol/L of Ang II, because the distance from the surface of the preparation to the RVLM neurons makes it difficult for Ang II to reach the target neurons.

We then performed superfusion with a mixture of Ang II (6 μmol/L) and tetrodotoxin (50 μmol/L; Wako Pure Chemical Industries). Tetrodotoxin was used to block every synaptic input to the RVLM neurons. The intermediolateral cell column neurons were stimulated with a stainless-steel electrode (5 to 15 V, 100 ms, single pulse) to identify the RVLM bulbospinal neurons. RVLM bulbospinal neurons showing antidromic action potentials after intermediolateral cell column stimulation were used in the experiments.[17] Lucifer yellow was allowed to diffuse spontaneously or by iontophoresis into the neurons during the intracellular recordings to verify the location of the neurons examined.[18] All of the data were recorded and analyzed using PowerLab (AD Instruments). After the addition of tetrodotoxin, we first confirmed the disappearance of phrenic nerve activity (≈15 to 20 minutes after the addition of tetrodotoxin) and then added Ang II to the superfusate. Superfusion with Ang II induced depolarization in the bulbospinal neurons of the RVLM after a 1- or 2-minute latency period.

Statistics

All of the data were represented as the means±SDs. Differences between the WKY and WKYpch1.0 rats or between the SHRSP-wch1.0 and SHRSP rats were examined using independent t tests. A value of $P<0.05$ was considered statistically significant.

Results

Basal Electrophysiological Activities of the RVLM Neurons

The RVLM neurons are classified into 3 types: regularly firing neurons, irregularly firing neurons, and silent-type neurons; however, the physiological roles of these neurons have not yet been fully elucidated.[14] The irregularly firing neurons exhibited many excitatory postsynaptic potentials, whereas the regularly firing neurons rarely showed such behavior (Figures 1 and 2).

In the regularly firing neurons, the basal membrane potential was significantly less negative in the WKYpch1.0 rats (−46.4±2.3 mV) than in the WKY rats (−55.4±5.6 mV). The basal membrane potential of the SHRSPwch1.0 rats (−47.8±2.6 mV) was similar to that of the SHRSP rats (−45.4±3.6 mV). The firing rate did not differ between the WKYpch1.0 and WKY rats or between the SHRSPwch1.0 and SHRSP rats.

As shown in Figure 2, the same trend was observed in the irregularly firing neurons of the RVLM; the basal membrane potential was significantly less negative in the WKYpch1.0 rats (−49.3±3.0 mV) than in the WKY rats (−57.0±1.0 mV; $P<0.01$). The basal membrane potential of the SHRSP-wch1.0 rats (−51.3±3.2 mV) was similar to that of the SHRSP rats (−50.0±0.0 mV). The firing rate did not differ between the WKYpch1.0 and WKY rats or between the SHRSPwch1.0 and SHRSP rats.

The input resistance of the regularly and irregularly firing neurons was also not significantly different among the 4 strains (data not shown).

Response to Ang II

Superfusion with Ang II (6 μmol/L) induced depolarization in the bulbospinal neurons of the RVLM after a 1- or 2-minute latency period. Repolarization toward the basal level was then observed over the next 2 or 3 minutes; this repolarization was considered to represent the desensitization of the neurons. We, thus, quantified the magnitude of the maximal depolarization.

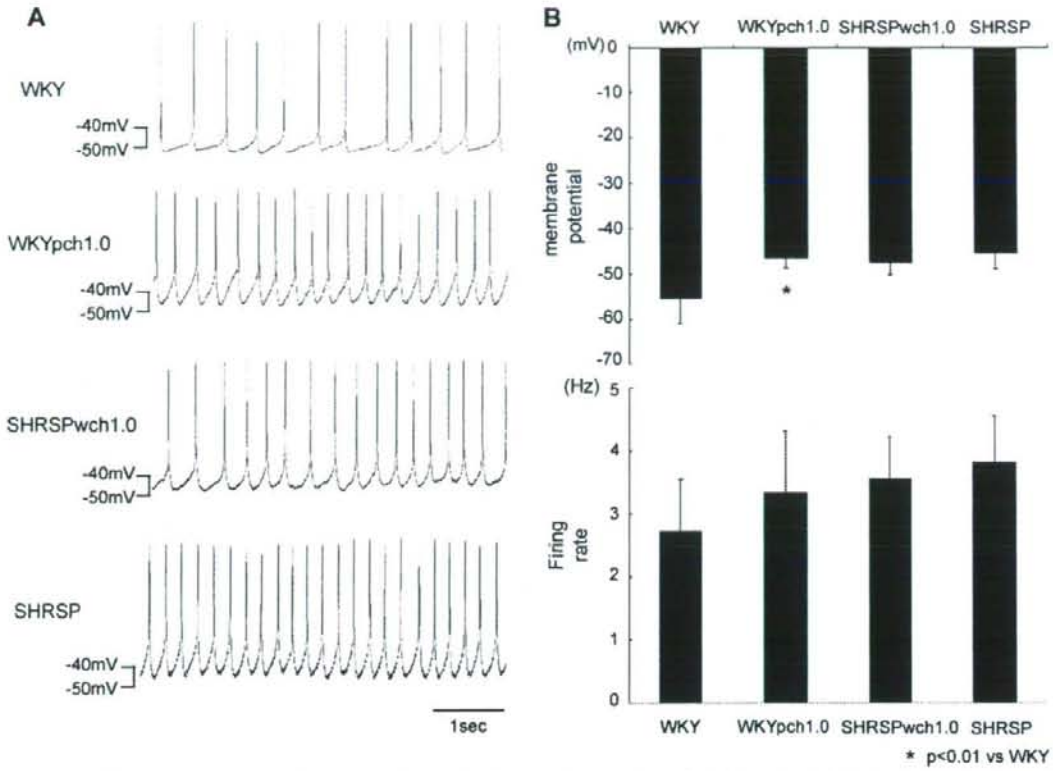

Figure 1. Basal membrane potential and firing rate of regularly firing neurons in the RVLM of 4 rat strains. A, Representative traces of neuronal activity in RVLM from the 4 strains, recorded using the intracellular whole-cell patch-clamp technique. B, Top and bottom panels show the basal membrane potential and the firing rate (mean±SD of 7 neurons from different rats of each strain).

The magnitude of the depolarization of the RVLM neurons from WKYpch1.0 rats during Ang II superfusion was +4.1±2.3 mV, which was significantly larger than that of the neurons from WKY rats (Figure 3). The depolarization of the RVLM neurons from SHRSPs was significantly larger than that of the neurons from SHRSPwch1.0 rats. Of note, the depolarization was statistically significant in the 2 strains (WKYpch1.0 and SHRSP) that possess the SHRSP-derived fragment of the Chr-1 QTL.

In the next experiment, which used a potent inhibitor of synaptic transmission, tetrodotoxin, we examined whether the Ang II effect was mediated through presynaptic or postsynaptic pathways. After the administration of tetrodotoxin, we first confirmed the disappearance of phrenic nerve activity and then added Ang II to the superfusate. The average magnitude of the depolarization of the neurons from WKYpch1.0 rats during superfusion with tetrodotoxin and Ang II was significantly larger than that of the neurons from WKY rats (Figure 4). Meanwhile, the average magnitude of the depolarization of the neurons from SHRSPs was also significantly larger than that of the neurons from SHRSPwch1.0 rats. These differences in depolarization were basically the same as those obtained in the experiments without tetrodotoxin, and the neurons from SHRSPs and WKYpch1.0 rats showed a significantly greater depolarization than those from the respective counterpart rats.

Discussion

The major finding of the present study was that the QTL on rat Chr-1 affected the electrophysiological activity of RVLM neurons, particularly their responsiveness to Ang II. Because isolated brain stem-spinal cord preparations from neonatal rats were used in this study, we would like to emphasize that the results were not caused by the secondary effects of hypertension or by the influence of the higher brain centers, such as the hypothalamus. Therefore, this observation strongly suggests that a gene (or genes) responsible for the difference in the activity of the RVLM neurons is (are) located in this genomic region.

In regularly firing neurons, the basal membrane potential differed significantly between neurons from WKY and WKYpch1.0 rats (Figure 1). Considering the genomic composition of the congenic strain (WKYpch1.0), this observation suggests that genes responsible for this interstrain difference are located both inside and outside of the QTL. Furthermore, the lack of a difference between neurons from SHRSPs and SHRSPwch1.0 rats implies that the effects of these genes are not additive, suggesting that they may be

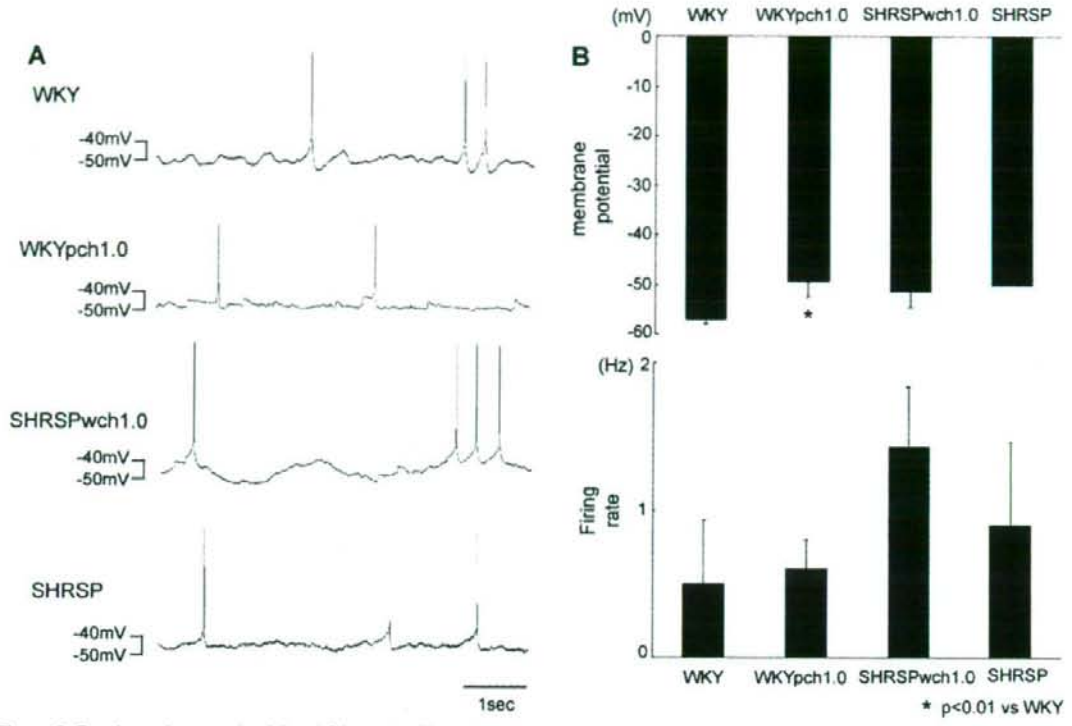

Figure 2. Basal membrane potential and firing rate of irregularly firing neurons in the RVLM. A, Representative traces from the 4 strains. B, Top and bottom panels show the basal membrane potential and the firing rate (mean±SD of 8 neurons from different rats).

involved in the same biological process, just as in the case of the blood pressure QTLs in Dahl salt-sensitive rats.[19]

In the irregularly firing neurons, we obtained a similar result regarding the difference in the basal membrane potential and no differences in the firing rate (Figure 2). These results can probably be explained by the fact that a larger number of synaptic inputs modulates the firing rate in irregularly firing neurons.[14] Nevertheless, a similar interstrain difference in the membrane potential was observed in neurons with different properties, suggesting that this genetic effect is ubiquitous in RVLM neurons.

The Ang II–induced depolarization and increase in the firing rate are shown in Figure 3. Of particular importance, these responses depended largely on the genotype of the congenic fragment, irrespective of the background genome; the 2 strains with the congenic fragment originating from SHRSPs (WKYpch1.0 and SHRSP) showed a significantly greater depolarization than the rats containing the congenic fragment originating from WKY rats (WKY and SHRSPwch1.0). This observation suggests that the responsiveness of the RVLM neurons to Ang II was largely determined by the gene(s) located in the QTL.

WKYpch1.0 rats have been shown repeatedly to have exaggerated sympathetic responses to different types of stress.[5–7] Considering a recent observation that the Ang II type 1 receptor in the RVLM mediates activating the sympathetic nervous system by emotional stress, resulting in an increase in blood pressure in conscious rabbits,[10] it is quite attractive to hypothesize that a gene (or genes) in the Chr-1 QTL affects (affect) the responsiveness of the sympathetic nervous system to stress through an Ang-II–mediated system in the RVLM. Supporting this hypothesis, Yamazato et al[7] reported that the hyperresponsiveness of blood pressure and renal sympathetic nerve activity to air-jet stress in WKYpch1.0 rats was inhibited by the intracerebroventricular injection of an Ang II receptor blocker.

Based on the results of the present study, we suspect that the basal membrane potential in RVLM neurons is affected primarily by age and background genome, whereas the response to Ang II in RVLM neurons depends on the blood pressure QTL of Chr-1. The depolarization of the RVLM neurons by Ang II superfusion was statistically significant in the neonatal WKYpch1.0 and SHRSPs but not in the neonatal WKY and SHRSPwch1.0 rats. Our data are supported by the results reported by Yamazato et al,[7] who showed that increases in renal sympathetic nerve activity in response to air-jet stress were significantly larger in 4-week–old WKYpch1.0 and SHRSPs than in 4-week–old WKY rats and that the sympathoexcitation of WKYpch1.0 rats was similar to that of SHRSPs. The depolarization of RVLM neurons by Ang II shown in our study may account for the increases in sympathetic nerve activity and blood pressure in response to air-jet stress, because the intracerebroventricular injection of Ang II receptor blocker candesartan reduced the sympatho-

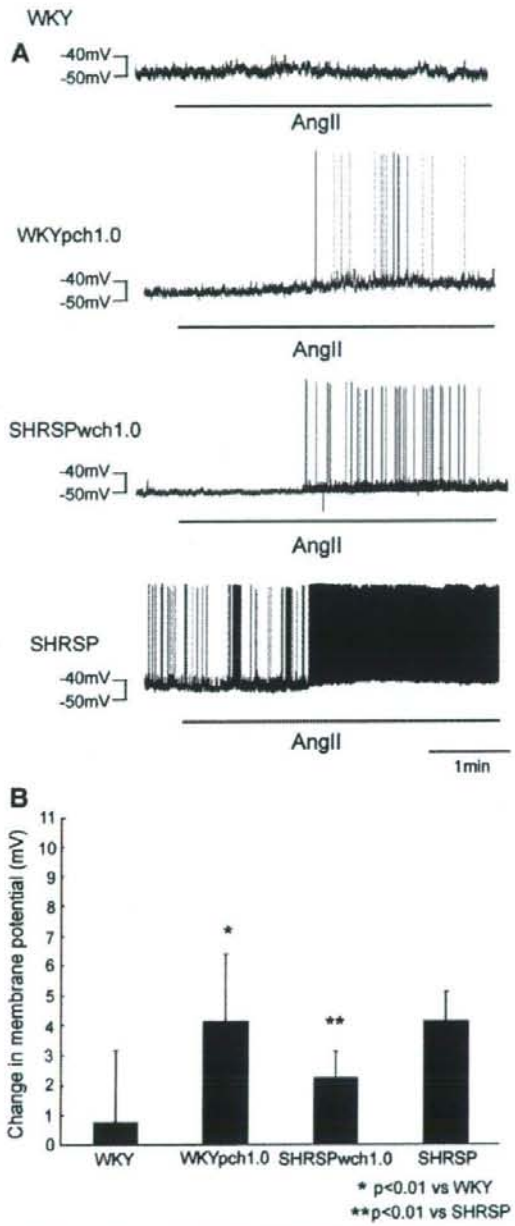

Figure 3. Effect of Ang II (6 μmol/L) superfusion on membrane potential of RVLM neurons. A, Representative traces from each strain. B, Changes in membrane potential (depolarization) in response to Ang II superfusion (mean±SD of 8 neurons from different rats of each strain).

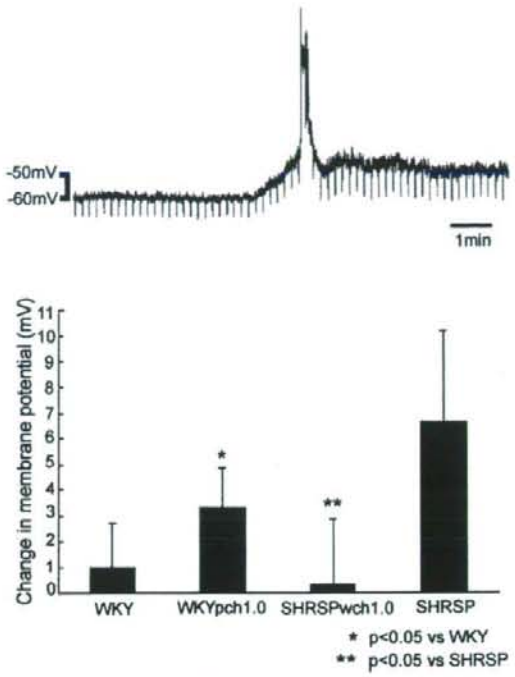

Figure 4. Top, Representative tracing of membrane potential in response to Ang II superfusion in the presence of tetrodotoxin during the application of a single current pulse (500 ms) for constructing a current-voltage (iv) curve every 10 seconds. A significant depolarization was detected as the result of a calcium influx through voltage-dependent calcium channels. Bottom, Changes in membrane potential in response to Ang II (6 μmol/L) superfusion in the presence of tetrodotoxin (50 μmol/L; mean±SD of 5 neurons from different rats).

excitatory and pressor responses.[7] Also, a report from Cui et al[5] demonstrated that the increase in systolic blood pressure in response to restraint stress in 16- to 20-week-old WKYpch1.0 rats was larger than that of WKY rats. These compatible data for different rat ages and from 3 different laboratories strongly suggest that the genes in the Chr-1 QTL of SHRSPs are responsible for the depolarization response of RVLM neurons to Ang II in neonatal WKYpch1.0 and SHRSPs, the increase in peripheral sympathetic activity in response to air-jet stress in 4-week-old WKYpch1.0 and SHRSPs, and the pressor response to restraint stress in 16- to 20-week-old WKYpch1.0 rats. However, these data do not suggest that age is responsible for the stress responses. In contrast, the basal blood pressures of WKY and WKYpch1.0 rats seem to be determined largely by age and also by genes both inside and outside the QTL.

In some cases, the effects of the QTL region on blood pressure were asymmetrical in reciprocal congenic strains for hypertensive QTLs. As Rapp[20] pointed out previously, strains with congenic fragments from the Dahl salt-sensitive rat on a background of normotensive strains did not show a significant increase in blood pressure, whereas congenic rats with the reversed genotype showed an obvious reduction. Consistent with this finding, WKYpch1.0 rats showed little, if any, increase in blood pressure, whereas SHRSPwch1.0 rats showed a large decrease.[3,13] This asymmetrical nature of the effects of QTLs on blood pressure was probably caused by gene-gene interactions, which convoluted the analyses. In

contrast, reciprocal genetic effects like the one observed in the present study suggest a mendelian control of phenotypes: the genotype (or the haplotype) of a single gene (or a cluster of genes) had a major effect on the phenotype, independent of the genetic background.[21,22] Such a phenotype may be regulated by the gene(s) in a more direct manner and may be useful for speculating the functions of the gene(s).

Because tetrodotoxin blocks all synaptic transmissions, the observation that the addition of tetrodotoxin did not change the responsiveness to Ang II further implied that the inter-strain difference in the responsiveness was intrinsic (or postsynaptic) in the RVLM neurons. A previous study of Sumners et al[23] reported that the exaggerated reactivity of RVLM neurons to Ang II in spontaneously hypertensive rats was because of an increase in the number of Ang II receptors on the RVLM neurons, which then induced oxidative stress and activated signal transduction via G proteins. It would be interesting to investigate the underlying intracellular mechanisms of the Ang II–dependent activation of RVLM neurons using congenic strains.

The blood pressure QTL on rat Chr-1 is quite large and contains hundreds of genes and expressed sequence tags.[5,13] Among them, however, several interesting candidates were found when the putative roles of the genes in the sympathetic nervous system were considered. These genes include Arix, a transcription factor regulating the development of the sympathetic nervous system, as well as the expression of dopamine β-hydroxylase[24–26]; Ntrk3, a receptor for neurotropin 3[27]; Arrb1, a cofactor regulating the internalization of the β-adrenergic receptors and angiotensin receptors[28]; Nox4, a subunit of NADPH oxidase[29]; and Homer 2, a regulator of the metabolic glutamate receptors.[30,31] In future studies, it will be necessary to reduce the number of candidate genes using both their positional and functional information to identify the responsible gene(s) and to confirm the roles of increased RVLM activity in the pathogenesis of hypertension.

The main limitation of this study is the lack of data regarding how RVLM neuron activity may (or may not) differ between strains in older animals and how this possible difference may be correlated with blood pressure. We hope to measure the RVLM neuron activity of both young and old rats in the future. To demonstrate that these early differences in RVLM neuron activity are causally related to stress-related differences in blood pressure, we should have compared the RVLM activity of older congenic and parental rats. Ideally, the electrophysiological properties of RVLM and the blood pressure, heart rate, and renal sympathetic nerve activity should be simultaneously examined in neonatal and older rats in vivo, and the changes in these parameters in response to various stressors should be determined. However, because the contact between the targeted neurons and the patch pipette is impaired by the increase in glial cells and astrocytes that occurs in rats older than 2 weeks of age, intracellular patch-clamp recordings of RVLM neurons are technically impossible to perform in older rats.

Perspectives

Several lines of evidence have indicated that sympathetic nerve activity differs significantly between spontaneously hypertensive rats/SHRSPs and WKY rats, and this difference is one of the putative causes of hypertension in spontaneously hypertensive rats/SHRSPs. Because membrane potential of RVLM neurons determines the sympathetic tone, the present observation suggests that a gene (or genes) in the Chr-1 QTL is (are) responsible for the greater sympathetic tone observed in SHRSPs. Identification of the responsible gene(s) will improve our understanding of the role of the sympathetic nervous system in the pathogenesis of hypertension and promote the development of new therapeutic and preventive strategies for essential hypertension.

Sources of Funding

This work was supported by Grants-in-Aid for Scientific Research from the Ministry of Education, Science and Culture of Japan.

Disclosures

None.

References

1. Okamoto K, Yamori Y, Nagaoka A. Establishment of the stroke-prone spontaneously hypertensive rat (SHR). *Circ Res*. 1974;34/35:I-143–I-153.
2. Mashimo T, Nabika T, Matsumoto C, Tamada T, Ueno K, Sawamura M, Ikeda K, Kato N, Nara T, Yamori Y. Aging and salt-loading modulate blood pressure QTLs in rats. *Am J Hypertens*. 1999;12:1098–1104.
3. Kato N, Mashimo T, Nabika T, Cui ZH, Ikeda K, Yamori Y. Genome-wide searches for blood pressure quantitative trait loci in the stroke-prone spontaneously hypertensive rat of a Japanese colony. *J Hypertens*. 2003;21:295–303.
4. Kato N, Nabika T, Liang Y-Q, Mashimo T, Inomata H, Watanabe T, Yanai K, Yamori Y, Yazaki Y, Sasazuki T. Isolation of a chromosome 1 region affecting blood pressure and vascular disease traits in the stroke-prone rat model. *Hypertension*. 2003;42:1191–1197.
5. Cui ZH, Ikeda K, Kawakami K, Gonda T, Nabika T, Masuda J. Exaggerated response to restraint stress in rats congenic for the chromosome 1 blood pressure quantitative trait locus. *Clin Exp Pharmacol Physiol*. 2003;30:464–469.
6. Cui ZH, Ikeda K, Kawakami K, Gonda T, Masuda J, Nabika T. Exaggerated response to cold stress in a congenic strain for the quantitative trait locus for blood pressure. *J Hypertens*. 2004;22:2103–2109.
7. Yamazato M, Ohya Y, Nakamoto M, Sakima A, Tagawa T, Harada Y, Nabika T, Takishita S. Sympathetic hyperreactivity to air-jet stress in the chromosome 1 blood pressure quantitative trait locus congenic rats. *Am J Physiol Regul Integr Comp Physiol*. 2006;290:R709–R714.
8. Dampney RA, Tan PS, Sheriff MJ, Fontes MA, Horiuchi J. Cardiovascular effects of angiotensin II in the rostral ventrolateral medulla: the push-pull hypothesis. *Curr Hypertens Rep*. 2007;9:22–27.
9. Guyenet PG, Haselton JR, Sun MK. Sympathoexcitatory neurons of the rostroventrolateral medulla and the origin of the sympathetic vasomotor tone. *Prog Brain Res*. 1989;81:105–116.
10. Mayorov DN, Head GA. AT1 receptors in the RVLM mediate pressor responses to emotional stress in rabbits. *Hypertension*. 2003;41:1168–1173.
11. Matsuura T, Kumagai H, Kawai A, Onimaru H, Imai M, Oshima N, Sakata K, Saruta T. Rostral ventrolateral medulla neurons of neonatal Wistar-Kyoto and spontaneously hypertensive rats. *Hypertension*. 2002;40:560–565.
12. Serikawa T. Colourful history of Japan's rat resources. *Nature*. 2004;429:15.
13. Yao H, Cui ZH, Masuda J, Nabika T. Congenic removal of a QTL for blood pressure attenuates infarct size produced by middle cerebral artery occlusion in hypertensive rats. *Physiol Genomics*. 2007;30:69–73.
14. Oshima N, Kumagai H, Kawai A, Sakata K, Matsuura T, Saruta T. Three types of putative presympathetic neurons in the rostral ventrolateral medulla studied with rat brainstem-spinal cord preparation. *Auton Neurosci*. 2000;84:40–49.
15. Onimaru H, Homma I. Whole cell recording from respiratory neurons in the medulla of brainstem-spinal cord preparations isolated from newborn rats. *Pflugers Arch Eur J Physiol*. 1992;420:399–406.

16. Li Y-W, Guyenet PG. Angiotensin II decreases a resting K+ conductance in rat bulbospinal neurons of the C1 area. *Circ Res*. 1996;78:274–282.
17. Iigaya K, Kumagai H, Onimaru H, Kawai A, Oshima N, Onami T, Takimoto C, Kamayachi T, Hayashi K, Saruta T, Itoh H. Novel axonal projection from the caudal end of the ventrolateral medulla to the intermediolateral cell column. *Am J Physiol Regul Integr Comp Physiol*. 2007;292:R927–R936.
18. Paxinos G, Watson C. *The Rat Brain in Stereotaxic Coordinates*. 2nd ed. Sydney, Australia: Academic Press; 1986.
19. Charron S, Duong C, Menard A, Roy J, Eliopoulos V, Lambert R, Deng AY. Epistasis, not numbers, regulates functions of clustered Dahl rat quantitative trait loci applicable to human hypertension. *Hypertension*. 2005;46:1300–1308.
20. Rapp JP. Genetic analysis of inherited hypertension in the rat. *Physiol Rev*. 2000;80:135–172.
21. Nabika T, Kobayashi Y, Yamori Y. Congenic rats for hypertension: how useful are they for the hunting of hypertension genes? *Clin Exp Pharmacol Physiol*. 2000;27:251–256.
22. Wang T, Nabika T, Notsu Y, Takabatake T. Sympathetic regulation of the renal functions in rats reciprocally congenic for chromosome 1 blood pressure quantitative trait locus. *Hypertens Res*. 2008;31:561–568.
23. Sumners C, Fleegal MA, Zhu M. Angiotensin AT1 receptor signaling pathways in neurons. *Clin Exp Pharmacol Physiol*. 2002;29:483–490.
24. Yang C, Kim HS, Seo H, Kim CH, Brunet JF, Kim KS. Paired-like homeodomain proteins, Phox2a and Phox2b, are responsible for noradrenergic cell-specific transcription of the dopamine beta-hydroxylase gene. *J Neurochem*. 1998;71:1813–1826.
25. Swanson DJ, Zellmer E, Lewis EJ. The homeodomain protein Arix interacts synergistically with cyclic AMP to regulate expression of neurotransmitter biosynthetic genes. *J Biol Chem*. 1997;272:27382–27392.
26. Morin X, Cremer H, Hirsch MR, Kapur RP, Goridis C, Brunet JF. Defects in sensory and autonomic ganglia and absence of locus coeruleus in mice deficient for the homeobox gene phox2a. *Neuron*. 1997;18:411–423.
27. ElShamy WM, Linnarsson S, Lee KF, Jaenisch R, Ernfors P. Prenatal and postnatal requirements of NT-3 for sympathetic neuroblast survival and innervation of specific targets. *Development*. 1996;122:491–500.
28. DeFea K. Beta-arrestins and heterotrimeric G-proteins: collaborators and competitors in signal transduction. *Br J Pharmacol*. 2008;153:s298–s309.
29. Dai X, Cao X, Kreulen DL. Superoxide anion is elevated in sympathetic neurons in DOCA-salt hypertension via activation of NADPH oxidase. *Am J Physiol*. 2006;290:H1019–H1026.
30. Ehrengruber MU, Kato A, Inokuchi D, Hennou S. Homer/Vesl proteins and their roles in CNS neurons. *Mol Neurobiol*. 2004;29:213–227.
31. Hinojos CA, Boerwinkle E, Fornage M, Eoris PA. Combined genealogical, mapping, and expression approaches to identify SHR hypertension genes. *Hypertension*. 2005;45:698–704.

Journal of Translational Medicine BioMed Central

Research

Open Access

Transplantation of vascular cells derived from human embryonic stem cells contributes to vascular regeneration after stroke in mice

Naofumi Oyamada[1], Hiroshi Itoh*[2], Masakatsu Sone[1], Kenichi Yamahara[1], Kazutoshi Miyashita[2], Kwijun Park[1], Daisuke Taura[1], Megumi Inuzuka[1], Takuhiro Sonoyama[1], Hirokazu Tsujimoto[1], Yasutomo Fukunaga[1], Naohisa Tamura[1] and Kazuwa Nakao[1]

Address: [1]Department of Medicine and Clinical Science, Kyoto University Graduate School of Medicine, Japan Department of Medicine and Clinical Science, Kyoto University Graduate School of Medicine, 54 Shogoin Kawahara-cho, Sakyo-ku, Kyoto, 606-8507, Japan and [2]Department of Internal Medicine, Keio University School of Medicine 35 Shinanomachi, Shinjuku-ku Tokyo 160-8582, Japan

Email: Naofumi Oyamada - kanu@kuhp.kyoto-u.ac.jp; Hiroshi Itoh* - hrith@sc.itc.keio.ac.jp; Masakatsu Sone - sonemasa@kuhp.kyoto-u.ac.jp; Kenichi Yamahara - yamahara@kuhp.kyoto-u.ac.jp; Kazutoshi Miyashita - miyakaz@sc.itc.keio.ac.jp; Kwijun Park - takanori@kuhp.kyoto-u.ac.jp; Daisuke Taura - dai12@kuhp.kyoto-u.ac.jp; Megumi Inuzuka - inuzukam@kuhp.kyoto-u.ac.jp; Takuhiro Sonoyama - sonoyama@kuhp.kyoto-u.ac.jp; Hirokazu Tsujimoto - tsujis51@kuhp.kyoto-u.ac.jp; Yasutomo Fukunaga - fukuyasu@kuhp.kyoto-u.ac.jp; Naohisa Tamura - ntamura@kuhp.kyoto-u.ac.jp; Kazuwa Nakao - nakao@kuhp.kyoto-u.ac.jp

* Corresponding author

Published: 30 September 2008

Journal of Translational Medicine 2008, 6:54 doi:10.1186/1479-5876-6-54

Received: 22 May 2008
Accepted: 30 September 2008

This article is available from: http://www.translational-medicine.com/content/6/1/54

Abstract

Background: We previously demonstrated that vascular endothelial growth factor receptor type 2 (VEGF-R2)-positive cells induced from mouse embryonic stem (ES) cells can differentiate into both endothelial cells (ECs) and mural cells (MCs) and these vascular cells construct blood vessel structures in vitro. Recently, we have also established a method for the large-scale expansion of ECs and MCs derived from human ES cells. We examined the potential of vascular cells derived from human ES cells to contribute to vascular regeneration and to provide therapeutic benefit for the ischemic brain.

Methods: Phosphate buffered saline, human peripheral blood mononuclear cells (hMNCs), ECs-, MCs-, or the mixture of ECs and MCs derived from human ES cells were intra-arterially transplanted into mice after transient middle cerebral artery occlusion (MCAo).

Results: Transplanted ECs were successfully incorporated into host capillaries and MCs were distributed in the areas surrounding endothelial tubes. The cerebral blood flow and the vascular density in the ischemic striatum on day 28 after MCAo had significantly improved in ECs-, MCs- and ECs+MCs-transplanted mice compared to that of mice injected with saline or transplanted with hMNCs. Moreover, compared to saline-injected or hMNC-transplanted mice, significant reduction of the infarct volume and of apoptosis as well as acceleration of neurological recovery were observed on day 28 after MCAo in the cell mixture-transplanted mice.

Conclusion: Transplantation of ECs and MCs derived from undifferentiated human ES cells have a potential to contribute to therapeutic vascular regeneration and consequently reduction of infarct area after stroke.

Background

Stroke, for which hypertension is the most important risk factor, is one of the common causes of death and disability in humans. It is widely considered that stroke patients with a higher cerebral blood vessel density show better progress and survive longer than patients with a lower vascular density. Angiogenesis, which has been considered to the growth of new capillaries by sprouting of preexisting vessels through proliferation and migration of mature endothelial cells (ECs), plays a key role in neovascularization. Various methods for therapeutic angiogenesis, including delivery of angiogenic factor [1,2] or cell transplantation [3-5], have been used to induce collateral blood vessel development in several animal models of cerebral ischemia. More recently, an alternative paradigm, known as postnatal vasculogenesis, has been shown to contribute to some forms of neovascularization. In vasculogenesis, endothelial progenitor cells (EPCs), which have been recognized as cellular components of the new vessel structure and reserved in the bone marrow, can take an important part in tissue neovascularization after ischemia [6]. Previous reports demonstrated that transplantation of mouse bone marrow cells after cerebral ischemia increased the cerebral blood flow partially via the incorporation of EPCs into host vascular structure as vasculogenesis [4]. However, because the population of EPCs in the bone marrow and in the peripheral blood has been revealed to be very small [7], it is now recognized to be difficult to prepare enough EPCs for the promotion of therapeutic vaculogenesis after ischemia.

We previously demonstrated that VEGF-R2-positive cells induced from undifferentiated mouse embryonic stem (ES) cells can differentiate into both VE-cadherin-positive endothelial cells (ECs) and αSMA-positive mural cells (MCs), and these vascular cells construct blood vessel structures [8]. We have also succeeded that after the induction of differentiation on OP9 feeder layer, VEGFR-2-positive cells derived from not only monkey ES cells [9] but human ES cells [10], effectively differentiated into both ECs and MCs. Next, we demonstrated that VE-cadherin$^+$VEGF-R2$^+$TRA-1$^-$cells differentiated from human ES cells on day 10 of differentiation, which can be considered as ECs in the early differentiation stage, could be expanded on a large scale to produce enough number of ECs for transplantation [10]. Moreover, we also succeeded in expanding not only ECs but also MCs derived from these ECs in the early differentiation stage in vitro.

In the present study, we examined whether ECs and MCs derived from human ES cells could serve as a source for vasculogenesis in order to contribute to therapeutic neovascularization and to neuroprotection in the ischemic brain.

Methods

Preparation of human ECs and/or MCs derived from human ES cells

Maintenance of human ES cell line (HES-3) was described previously [10]. We plated small human ES colonies on OP9 feeder layer to induce differentiation into ECs and MCs [10]. On day 10 of differentiation, VE-cadherin$^+$VEGF-R2$^+$TRA-1$^-$ cells were sorted with a fluorescence activator cell sorter (FACSaria; Becton Dickinson). Monoclonal antibody for VEGF-R2 was labeled with Alexa-647 (Molecular Probes). Monoclonal antibody for TRA1-60 (Chemicon) was labeled with Alexa-488 (Molecular Probes) and anti VE-cadherin (BD Biosciecnces) antibody was labeled with Alexa 546 (Molecular Probes). After sorting the VE-cadherin$^+$VEGFR-2$^+$TRA-1$^-$ cells on day 10 of differentiation, we cultured them on type IV collagen-coated dishes (Becton Dickinson) with MEM in the presence of 10% fetal calf serum (FCS) and 50 ng/ml human VEGF165 (Peprotech) and expanded these cells. After five passages in culture (= approximately 30 days after the sorting), we obtained the expanded cells as a mixture of ECs and MCs derived from human ES cells (hES-ECs+MCs). The cell mixture was composed of almost the same number of ECs and MCs. We resorted the VE-cadherin$^+$ cells from these expanded cells to obtain ECs for transplantation (Figure 1). The ECs derived from human ES cells (hES-ECs) were labeled with CM-Dil (Molecular Probes) before the transplantation.

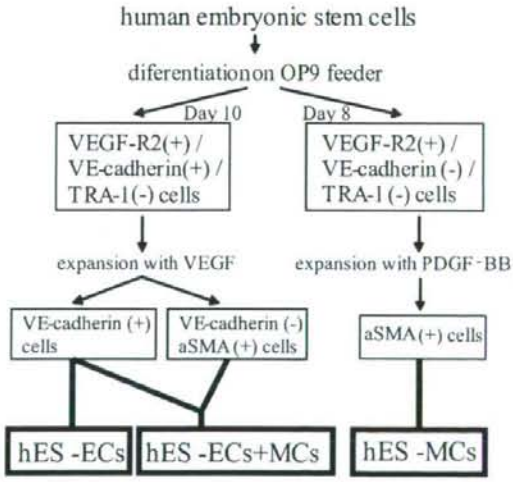

Figure 1
Schematic representation of preparation of the transplanted vascular cells differentiated from human ES cells.

After sorting VE-cadherin$^+$VEGFR-2$^+$TRA-1$^-$ cells on day 8 of differentiation, we cultured these cells on type IV collagen-coated dishes by five passages (= approximately 40 days after the sorting) in the presence of 1% FCS and PDGF-BB (10 ng/ml) (PeproTech) to obtain only MCs derived from human ES cells (hES-MCs) for the transplantation (Figure 1). On the day of transplantation, these cells were washed with PBS twice and harvested with 0.05% trypsin and 0.53 mmol/L EDTA (GIBCO) for 5 minutes. Each cells used for the transplantation was suspended in 50 ul PBS.

Preparation of human mononuclear cells

We performed the transplantation of human mononuclear cells (hMNCs), which contain a very small population of EPCs (≦ 0.02%) [7], to examine the non-specific influences due to the cell transplantation itself. The hMNCs were prepared from 10 ml samples of peripheral blood of healthy volunteers. Each sample was diluted twice with PBS and layered over 8 ml of Ficoll (Biosciences). After centrifugation at 2500 g for 30 minutes, the mononuclear cell layer was harvested in the interface and resuspended in PBS (3×10^6 cells/50 ul) for the transplantation.

Immunohistochemical examination of cultured cells

Staining of cultured cells on dishes at 5th passage was performed as described elsewhere [8,10]. Monoclonal antibodies for alpha smooth muscle actin (αSMA) (Sigma), human CD 31 (BD Biosciecnces) and calponin (Dako Cytomation) were used.

Middle cerebral artery occlusion (MCAo) model and cell transplantation

We used adult male C57 BL6/J mice weighing 20–25 g for all our experiments, and all of them were anesthetized with 5% halothane and maintained 1% during the experiments. We induced transient left middle cerebral artery occlusion (MCAo) for 20 min as previously described [11]. Briefly, a 8-0 nylon monofilament coated with silicone was inserted from the left common carotid artery (CCA) via the internal carotid artery to the base of the left MCA. After the occlusion for 20 minutes, the filament was withdrawn and intra-arterial injection of hES-derived vascular cells was performed through the left CCA. We prepared four groups of the transplanted cells; Group1: PBS (50 ul), Group 2: hMNCs (3×10^6 cells), Group 3: hES-ECs (1.5×10^6 cells), Group 4: hES-MCs (1.5×10^6 cells), Group 5: hES-ECs+MCs (3×10^6 cells). After transplantation, the distal portion of CCA was ligated. All animals were immunosuppressed with cyclosporin A (4 mg/kg, ip) on day 1 before the transplantation, postoperative day 1–7, 10, 14, and 21. Experimental procedures were performed in accordance with Kyoto University guidelines for animal experiments.

Assessment for cerebral blood flow after the transplantation

We measured the cerebral blood flow (CBF) just before the experiments (= day 0) and on day 4 and 28 after MCAo by mean of a Laser-Doppler perfusion imager (LDPI, Moor Instruments Ltd.). During the measurement, each mouse was anesthetized with halothane and the room temperature was kept at 25–27°C. The ratio of blood flow of the area under MCA in the ipsilateral side to the contralateral side was calculated as previously described [11].

Immunohistochemical examination of the ischemic striatum

The harvested brains were subjected to immunohistochemical examination using a standard procedure as previously described [12]. In all of our examination, free-floating 30-μm coronal sections at the level of the anterior commisure (= the bregma) were stained and examined with a confocal microscope (LSM5 PASCAL, Carl Zeiss). Sections were subjected to immunohistochemical analysis with the antibodies for human PECAM-1 (BD Biosciecnces, 1:100), mouse PECAM-1 (BD Bioscience, 1:100), human HLA-A, B, C (BD Biosciecnces, 1:100), αSMA (BD Biosciecnces, 1:100), Neu-N (Chemicon, 1:200), and single stranded DNA (Dako Cytomation, 1:100).

In our model of MCAo, the infarct area was confined to the striatum. The ischemic striatum at the level of the anterior commisure from each mouse was photographed on day 28 after MCAo. The procedure of the quantification of vascular density was carried out as described in Yunjuan Sun et al. [13] with slight modification. Vascular density in the ischemic striatum was examined at ×20 magnification, by quantifying the ratio of the pixels of human and/or mouse PECAM-1-positive cells to 512 × 512 pixels in that field: the ratio was expressed as %area. The number of transplanted MCs detected in the ischemic core at ×20 magnification was calculated. To identify localization of transplanted ECs or MCs, the fields in the ischemic striatum were photographed at ×63 magnification. The infarct area (mm^2/field/mouse) at the level of the bregma was defined and quantified as the lesion where Neu-N immunoreactivity disappeared in the striatum at ×5 magnification as previously described [11,14]. The measurement of infarct volumes was carried out as described in Sakai T. et al. [14] with slight modification. Another saline- and EC+MC-injected groups were sacrificed on day 28 after MCAo. For the measurements of the infarct volume, 5 coronal sections (approximately -1 mm, -0.5 mm, ± 0 mm, +0.5 mm and +1 mm from the bregma) were prepared from each mouse and each infarct area (mm^2) was measured. And then, the infarct area was summed among slices and multiplied by slice thickness to provide infract volume (mm^3). To calculate apoptotic

cells, the number (cells/mm²/mouse) of single stranded DNA (ss-DNA)⁺ cells in one field in the ischemic core from each mouse in the saline- or hES-ECs+MCs-injected group was quantified at ×20 magnification on day 14 after MCAo.

Neurological Functional test

We used the rota-rod exercise machine for the assessment of the recovery of impaired motor function after MCAo. This accelerating rota-rod test was carried out as described in A.J. Hunter et al. [15] with slight modification. Each mouse was trained up to be able to keep running on the rotating rod over 60 seconds at 9 round per minutes (rpm) (2th speed). After the training was completed, we placed each mouse on the rod and changed the speed of rotation every 10 seconds from 6 rpm (1st speed) to 30 rpm (5th speed) over the course of 50 seconds and checked the time until the mouse fell off. The exercise time (seconds) on the rota-rod for each mouse was recorded just before the experiments (= day 0) and on day 7 and 28 after MCAo.

Analysis of mRNA expression of angiogenic factors

Cultured human aortic smooth muscle cells (hAoSMC) (Cambrex, East Rutherford, NJ) were used for control. Total cellular RNA was isolated from hES-MCs and human aortic smooth muscle cells (hAoSMC) (Cambrex, East Rutherford, NJ) with RNAeasy Mini Kit (QIAGEN K.K., Tokyo, Japan). The mRNA expression was analyzed with One Step RNA PCR Kit (Takara, Out, Japan). The primers used were as follows: human vascular endothelial growth factor (VEGF, Genbank accession No.X62568), 5'-AGGGCAGAATCATCACGAAG-3' (forward) and 5'-CGCTCCGTCGAACTCAATTT-3' (reverse); human basic fibroblast growth factor (bFGF, Genbank accession No.M27968), AGAGCGACCCTCACATCAAG (forward) and TCGTTTCAGTGCCACATACC (reverse); human hepatic growth factor (HGF, Genbank accession No.X16323), 5'-AGTCTGTGACATTCCTCAGTG-3' (forward) and 5'-TGAGAATCCCAACGCTGACA-3' (reverse); human platelet-derived growth factor (PDGF-B, Genbank accession No.X02811), 5'-GCACACGCATGACAA-GACGGC-3' (forward) and 5'-AGGCAGGCTATGCTGA-GAGGTCC-3' (reverse); and GAPDH (Genbank accession No.M33197), 5'-TGCACCACCAACTGCTTAGC-3' (forward) and 5'-GGCATGGACTGTGGTCATGA-3' (reverse). Polymerase chain reactions (PCR) were performed as described in the manufacturer's protocols.

Measurement of angiogenic factors in hES-MCs-conditioned media

After 1 × 10^6 cells of hES-MC or hAoSMC were plated on 10 cm type IV collagen-coated dishes and incubated with 5 ml media (αMEM with 0.5% bovine serum) for 72 hours, the concentration of human VEGF, bFGF and HGF were measured by SRL, Inc. (Tokyo, Japan).

Statistical analysis

All data were expressed as mean ± standard error (S.E.). Comparison of means between two groups was performed with Student's t test. When more than two groups were compared, ANOVA was used to evaluate significant differences among groups, and if there were confirmed, they were further examined by means of multiple comparisons. Probability was considered to be statistically significant at $P < 0.05$.

Results

Preparation and characterization of transplanted cells derived from human ES cells

We induced differentiation of human ES cells in an in vitro two-dimensional culture on OP9 stromal cell line and examined the expression of VEGF-R2, VE-cadherin and TRA-1 during the differentiation. While the population of VE-cadherin⁺VEGF-R2⁺TRA-1⁻ cells was not detected (< 0.5%) before day 8 of differentiation, it emerged and accounted for about 1–2% on day10 of differentiation (Figure 2A). As we previously reported, these VE-cadherin⁺VEGF-R2⁺TRA-1⁻ cells on day 10 of differentiation were also positive for CD34, CD31 and eNOS [10]. Therefore, we used the term 'eEC' for these ECs in the early differentiation stage. We sorted and expanded these eECs in vitro. These eECs were cultured in the presence of VEGF and 10% FCS and expanded by about 85-fold after 5 passages. The expanded cells at 5th passage were constituted with two cell fractions. One of these cells was VE-cadherin⁺ cells (35–50%), which were positive for other endothelial markers, including CD31 (Figure 2B–E) and CD34 [10], indicating that cell differentiation stage had been retained. The other was VE-cadherin⁻ cells (50–65%), which were positive for αSMA and considered to differentiate into MCs (Figure 2D–E). We sorted the fraction of VE-cadherin⁻VEGF-R2⁺TRA-1⁻ cells, which appeared on day 8 of differentiation and were positive for platelet derived growth factor receptor type β (PDGFR-β) [10], and expanded these cells for induction to MC in the presence of PDGF-BB and 1% FCS. At passage 5, all of the expanded cells effectively differentiated into αSMA-positive MCs (Figure 2F–G).

Assessment of cerebral blood flow recovery in the infarct area after the transplantation

As shown in Figure 3B, the cerebral blood flow in the ipsilateral side decreased by approximately 80% compared to that in the contralateral side during MCAo and the area with the suppressed blood flow was corresponded to the area under MCA. In the 5 groups, the CBF ratio on day 4 decreased by about 20% compared to that of the contralateral side due to ligation of the left CCA after the trans-

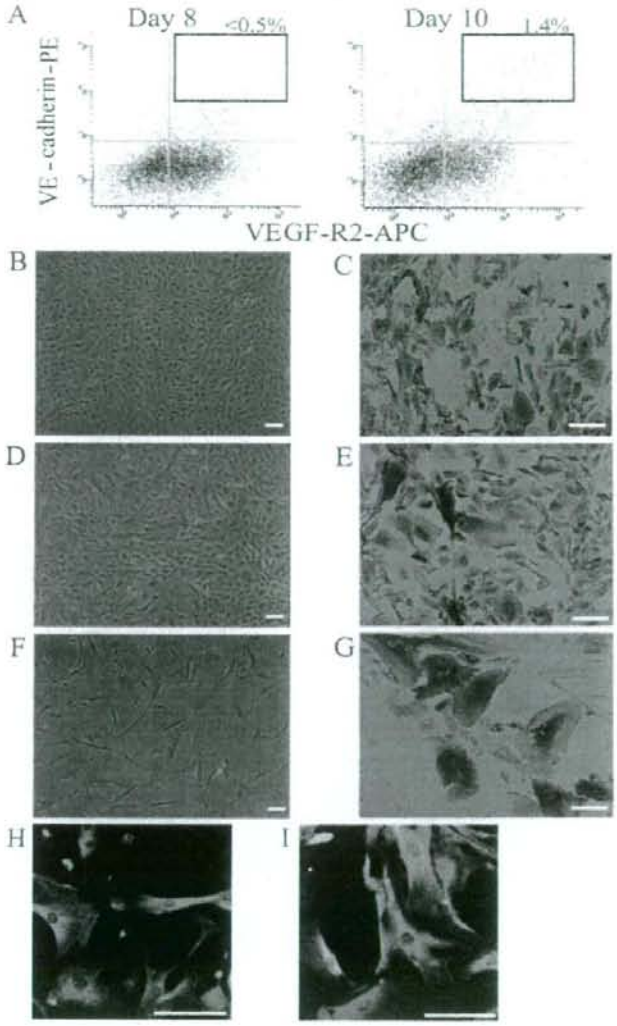

Figure 2

Characterization of the transplanted vascular cells derived from human ES cells (HES-3). A, Flow cytometric analysis of VE-cadherin and VEGF-R2 expression on human ES cells during differentiation on an OP9 feeder layer. VE-cadherin$^+$VEGF-R2$^+$TRA-1$^-$ cells are indicated by the boxed areas. B, Morphology of the VE-cadherin$^+$ cells (= hES-ECs) resorted from expanded VE-cadherin$^+$VEGF-R2$^+$TRA-1$^-$ cells at 5th passage. C, Immunostaining for human PECAM-1 (brown) of hES-ECs. D, Morphology of the expanded VE-cadherin$^+$VEGF-R2$^+$TRA-1$^-$ cells at 5th passage (= hES-ECs+MCs). E, Double immunostaining for human PECAM-1 (brown) and αSMA (purple) on hES-ECs+MCs. F, Morphology of the cells (= hES-MCs) expanded from VE-cadherin$^-$VEGF-R2$^+$TRA-1$^-$ cells on day 10 of differentiation with PDGF-BB and 1% FCS up to 5th passage. G, Immunostaining for αSMA (brown) of hES-MCs. H-I, Immunostaining for αSMA (green) and calponin (red) of hAoSMCs (H) and hES-MCs (I). Scale bar: 50 μm.

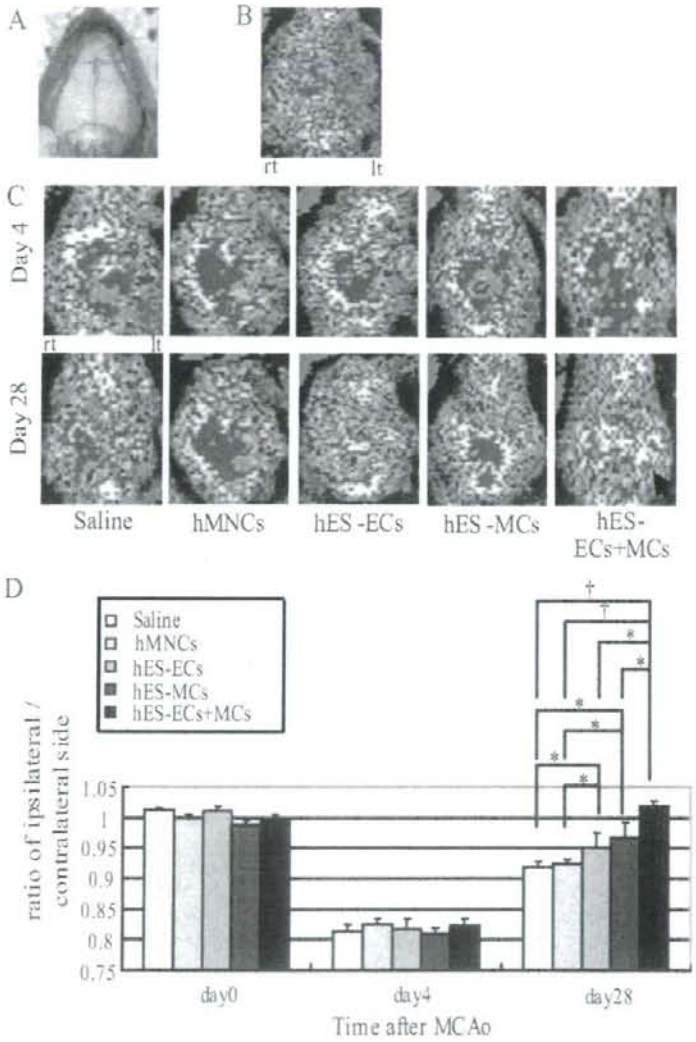

Figure 3

Effects of the transplanted vascular cells on the CBF in the ipsilateral side. A-C: LDPI analysis of the CBF by LDPI evaluated in mice with the scalp removed (A). Flowmetric analysis of the CBF in the ipsilateral side (= left side: lt) during MCA-occlusion (B). The CBF in the ipsilateral and contralateral side in the five groups on day 4 and 28 after MCAo (C). An arrow indicates the lesion in the hES-EC+MC-injected group where the CBF clearly increased up to or rather than the corresponding area in the contralateral side. Red or white indicates higher flow than blue or green. D, Quantitative analysis of the CBF ratio of the ipsilateral/contralateral side just before the experiments (= day 0) and on day 4 and 28 after MCAo. * $P < 0.05$, † $P < 0.01$.

plantation. Then, we assessed the recovery of the CBF in the ipsilateral side from this time point. Apparent difference in the CBF in the ipsilateral side was not observed among the 5 groups on day 4 after MCAo. However, the blood flow of the ipsilateral side in the hES-EC+MC-injected group, especially pointed out by the arrow, clearly increased up to or rather than the corresponding area in the contralateral side on day 28 after MCAo, compared to other 4 groups (Figure 3C). On day 28, the CBF ratio of the saline- and hMNC-injected group were similar (Figure 3D), while that of hES-EC-injected group increased significantly compared to that of these two groups (saline: 0.919 ± 0.010, n = 12. hMNCs: 0.925 ± 0.008, n = 15. hES-ECs: 0.952 ± 0.025, n = 7. $P < 0.05$). The CBF ratio of the hES-MC-injected group (0.968 ± 0.023, n = 7, $P < 0.05$) increased significantly compared to that of the saline- or hMNCs-injected groups on day 28, while that of the hES-EC+MC-injected group (1.018 ± 0.009: n = 13) increased significantly compared to not only that of the saline- or hMNCs-injected groups ($P < 0.001$), but also that of the hES-EC- or hES-MC-injected group ($P < 0.01$).

Localization of transplanted vascular cells derived from human ES cells and the vascular density in the infarct area after the transplantation

In the saline- and hMNCs-injected groups, the vascular density of host capillary quantified by mouse PECAM-1 immunoreactivity in the ischemic striatum (Figure 4B, C) was higher than that in the non-ischemic striatum (Figure 4A). In hMNCs-injected group, few human PECAM-1 positive cells were observed in the ischemic striatum (Figure 4C) and these cells were not found in the non-ischemic striatum. In the hES-EC-injected group, many DiI positive hES-ECs were observed in the infarct area (Figure 4D) and incorporated into the host capillaries (Figure 4E). In the hES-MC-injected group, both αSMA and human HLA positive cells (23.1 ± 2.0 counts/field: n = 7) were detected in the infarct area (Figure 4F) and localized in the conjunction with mouse endothelial tubes (Figure 4G). Compatible with these results, in the hES-EC+MC-injected group, many human PECAM-1 positive cells were detected in the host capillaries (Figure 4H) while transplanted MCs (21.7 ± 1.8 counts/field: n = 6) surrounded the capillaries in the infarct area, similarly to those in the hES-MCs-injected group (Figure 4I).

In the ischemic striatum, the density (%area) of human PECAM-1 positive cells was 0.05 ± 0.01% in the hMNC-injected group (n = 11), 0.66 ± 0.11% in the hES-EC-injected group (n = 7, $P < 0.0001$ vs hMNCs) and 0.85 ± 0.12% in the hES-EC+MC-injected group (n = 11, $P < 0.0001$ vs hMNCs) (Figure 5A). As shown in Figure 5B, there was no significant difference in the densities of mouse PECAM-1 positive cells among the saline- (10.3 ± 0.4%: n = 11), hMNC- (10.9 ± 0.3%: n = 11) and hES-EC- (11.4 ± 0.4%: n = 7) injected groups, although the densities were significantly higher than that in the non-ischemic striatum (5.6 ± 0.2%: n = 5). In hES-MC- (13.2 ± 0.5%: n = 7, $P < 0.01$ vs control, $P < 0.05$ vs hES-ECs) or hES-EC+MC- (13.8 ± 0.4%: n = 11, $P < 0.01$ vs control and hES-ECs) injected group, a significant increase in the density of mouse PECAM-1 positive cells was observed. The total vascular density estimated by summing up human and mouse PECAM-1 positive area (12.2 ± 0.6%, $P < 0.05$) in the hES-EC-injected group was significantly higher compared to that in the saline-injected group. Moreover, the total vascular density in the hES-EC+MC-injected group (14.7 ± 0.6%) was markedly higher compared to those in the other four groups ($P < 0.001$ vs control, $P < 0.01$ vs hES-ECs, $P < 0.05$ vs hES-MCs) (Figure 5C).

Analysis of the infarct size and apoptosis in the ipsilateral side after the transplantation

There was no significant difference in the infarct area in the striatum on day 28 after MCAo between the saline- (1.372 ± 0.041 mm^2: n = 10) and the hMNC- (1.438 ± 0.084 mm^2: n = 10) injected groups. The infarct area in the hES-EC- (1.308 ± 0.094 mm^2: n = 6) or the hES-MC- (1.249 ± 0.047 mm^2: n = 6) injected group showed a tendency to decrease. A significant decrease in the infarct area was observed in the hES-EC+MC-injected group (1.167 ± 0.085 mm^2: n = 9, $P < 0.05$) compared to the saline- and hMNCs-injected groups (Figure 6A, B). We also confined that the infarct volume was significantly reduced in the hES-EC+MC-injected group on day 28 after MCAo, compared to the saline-injected group (hES-EC+MC = 1.475 ± 0.083 mm^3: n = 9, saline = 1.736 ± 0.057 mm^3: n = 11, $P < 0.05$) (Figure 6C). On day 14 after MCAo, the number of ss-DNA^+ cells in the ischemic penumbral area in the hES-EC+MC-injected group (17.8 ± 2.5/mm^2: n = 5, $P < 0.05$) significantly decreased compared to that of the saline-injected group (43.5 ± 5.4/mm^2: n = 5) (Figure 6D, E).

Assessment of recovery of impaired motor function after MCAo

We estimated the exercise time by the rota-rod to evaluate the recovery of impaired motor function. Just before the experiment (day0) and on day 7 after MCAo, there was no significant difference of the exercise time in the 5 groups. Even on day 28 after MCAo, significant recovery of impaired motor function was not detected in the hES-EC- (31.2 ± 0.8 seconds, n = 7) or the hES-MC- (30.8 ± 0.7 seconds, n = 7) injected group, compared to that of the saline- (29.5 ± 1.2 seconds, n = 12) or hMNC- (30.1 ± 0.8 seconds, n = 15) injected group. On the other hand, we observed the improvement in the hES-EC+MC-injected group on day 28 after MCAo (33.1 ± 1.3 seconds, n = 13 vs saline or hMNC group: $P < 0.05$) (Figure 6F).

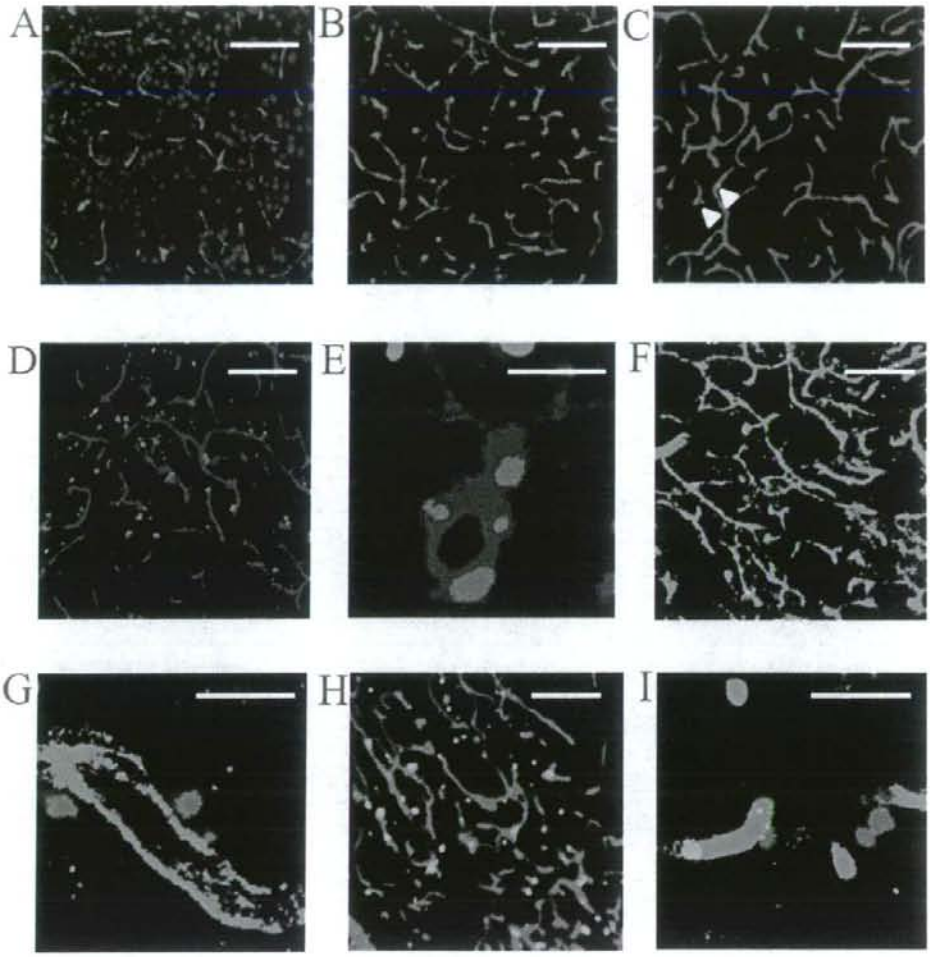

Figure 4 *(see previous page)*
Histological examination of the vasculature in the non-ischemic and ischemic striatum on day 28 after MCAo. A-C: Immunostaining of mouse PECAM-1 (red)/Neu-N (blue) in the non-ischemic striatum (A), and the ischemic striatum in saline (B)-and hMNC (C)-injected mice. Arrows show human PECAM-1$^+$ (green) cells in the ischemic striatum in the hMNC-injected group. D-E: Representative fluorescent photographs of the ischemic striatum stained for mouse PECAM-1 (blue), Neu-N (green) and CM-DiI (red) in hES-EC-injected mice. F-G: Immunostaining of αSMA (blue)/mouse PECAM-1 (green)/human HLA-A,B,C (red) in the ischemic striatum in the hES-MC-injected mice. Human HLA positive and αSMA positive hES-MCs were shown as purple (red+blue) cells. H, Immunostaining of mouse PECAM-1 (red)/Neu-N (blue)/human Pecam-1 (green) in the ischemic striatum in the hES-EC+MC-injected groups. I, Localization of transplanted hES-ECs+MCs in the ischemic striatum stained for αSMA (blue)/mouse PECAM-1 (green)/human HLA-A,B,C (red). A-D/F/H, scale bar: 100 μm, ×20 magnification. E/G/I, scale bar: 20 μm, ×63 magnification.